EXPERIMENTAL AND NUMERICAL INVESTIGATION OF POLYMERIC GYROID TPMS STRUCTURES UNDER CRUSHING LOAD

MATS OVERBECK[1,2], PIETRO BALLARIN[3], TIM LUPLOW[2] & SEBASTIAN HEIMBS[1,2]
[1]Cluster of Excellence SE^{2}A – Sustainable and Energy-Efficient Aviation,
Technische Universität Braunschweig, Germany
[2]Institute of Aircraft Design and Lightweight Structures (IFL), Technische Universität Braunschweig, Germany
[3]Department of Aerospace Science and Technology, Politecnico di Milano, Italy

ABSTRACT

Triply periodic minimal surface (TPMS) structures offer a unique set of characteristics that make them particularly attractive for aerospace applications. As open-cell structures with efficient specific strength and stiffness properties, they enable the design of lightweight and effective sandwich core materials for applications such as laminar flow control via boundary layer suction on the leading edge of an aircraft wing. In such components, bird strike often represents the critical load case for structural design, a precise understanding of the mechanical behaviour of TPMS structures is essential for their effective application in these contexts. Therefore, this study presents a comprehensive modelling methodology for gyroid structures integrating experimental and numerical methods to investigate both quasi-static and dynamic crushing behaviour. Initially, quasi-static coupon experiments are conducted on polymeric materials tailored for this application. Digital image correlation techniques are employed to analyse the stress states. Subsequently, dynamic tests are performed to assess the performance of TPMS structures under high loading rates. A finite element model is developed to simulate the mechanical response of the TPMS structures. This model is then validated against experimental data. The results demonstrate strong numerical–experimental agreement, with material parameters calibrated from coupon tests enabling an accurate representation of the stress–strain response and acceptable results were obtained for the first part of the dynamic crushing simulation of gyroid structures.
Keywords: TPMS, gyroid, compression, crushing, finite element modelling.

1 INTRODUCTION

Triply periodic minimal surface (TPMS) structures represent a viable solution to design and build aerospace structural elements, whose major requirement is represented by the weight, which must be as low as possible. Recently, some studies were presented by the Cluster of Excellence SE^{2}A – Sustainable and Energy-Efficient Aviation – and other research institutes about the application of such type of structures to the laminar flow control (LFC) with the purpose to reduce drag and the consequent fuel consumption delaying the laminar-turbulent transition [1]–[3]. Indeed, in the last years, the reduction of aircraft emissions has become more and more important to achieve sustainability since the aviation sector was responsible for 859 million tonnes of CO_2 in 2017 [4]. Moreover, from an economic standpoint, the expenses for fuel consumption represent 33.4% of the total cost of ownership (TCO) for an airline company [5]. The principle behind such concept consists in the suction of the boundary layer through the wing's outer skin. Indeed, previous studies demonstrated that a 45.5% of drag reduction can be obtained applying such a solution [6]. From an engineering standpoint, the solution can be implemented using porous wing panels supported by an internal porous core structure. A suction device is also needed to realise the air flow throughout the structure. The function of the porous filler can be performed by a TPMS structure, which is characterized by multiple cavities that allows the air to flow.

WIT Transactions on The Built Environment, Vol 215, © 2025 WIT Press
www.witpress.com, ISSN 1743-3509 (on-line)
doi:10.2495/SUSI250161

TPMS core structures also perform a structural role in addition to the aerodynamic one. The aircraft wing is subjected to different loads during flight. The leading edge plays a major role in aircraft safety. All parts oriented in flight direction can be subjected to bird strike loading, making this load case a design driving aspect. Therefore, the porous core needs to absorb a sufficient amount of the bird's kinetic energy to avoid damage to the wing's front spar. The front spar is one of the main load bearing parts of the aerodynamic loads. The structural integrity of the front spar and the wing box ensures a safe continuation of flight after a bird strike incident.

TPMS structures demonstrated excellent energy absorption capabilities [7], [8], which make them suitable for the aforementioned application. The implementation of LFC, and in particular the hybrid laminar flow control (HLFC), in which the boundary layer suction occurs also through the leading edge, requires the possibility to design and evaluate the structural strength and the energy absorption capability of the TPMS structures. Though a large number of experimental studies were carried out on the behaviour of TPMS structures [9]–[11], only few studies investigated the modelling strategies of such structures [12], [13].

In this work, different finite element (FE) modelling strategies are presented with the purpose to model the behaviour of TPMS structures, with focus on the gyroid type, in static and dynamic crushing conditions. The samples were produced by additive manufacturing in polymeric material. First, dogbone specimens were produced and experimentally tested under tensile loading to calibrate the material behaviour exploiting digital image correlation (DIC). Then, cubic specimens, representative of the gyroid structure, were manufactured and tested in static and dynamic compressive loading conditions. Different FE modelling approaches were compared based on the material's laws derived from the tests on the dogbone specimens.

This work is organized as follows: Section 2 describes the manufacturing process and the experimental methods adopted used in this study. Section 3 introduces the finite element modelling strategies. In Section 4, the numerical–experimental correlation is presented. Finally, Section 5 summarizes the main conclusions and outlines directions for future research.

2 EXPERIMENTS

This section outlines the methods adopted in this work to conduct the experimental part of the research activity. Specifically, in Subsection 2.1 the methodology to carry out the experiments and the manufacturing of the coupons is described, and in Subsection 2.2 the FE method to model the experiments is presented.

2.1 Manufacturing of the specimens

Two types of specimens were manufactured, the first type consisted of dogbone specimens, hereafter named specimen type A, which allowed calibrating the material model. The geometry is derived from the German norm DIN EN ISO 527-2 [14]. The second type of specimen consists of TPMS specimens, hereafter named specimens type B. The TPMS specimens are of a gyroid structure and cubic dimensions.

Specimens A were produced by additive manufacturing, using stereolithography technology. A Formlabs (Somervile) Form 3+ printer was used. A newly available photopolymer by Formlabs called Polyurethane Rigid 650 [15], which is characterized by great energy absorption properties according to the manufacturer was selected. This material is more challenging to manufacture compared to other SLA manufactured materials due to its tendency to interact with water. Therefore, the manufacturing process was conducted in a dry cabinet with a relative humidity below 5%. The material properties given by the manufacturer are presented in Table 1. The specimens were manufactured with a layer thickness of 50 μm. The printing orientation was varied in order to investigate any orientation dependency. Orientations of 0°, 45°, and 90° in respect to the printing platform were considered. The different printing orientations are depicted in Fig. 1. For each printing direction, six specimens were manufactured.

Table 1: Material properties of Formlabs Polyurethane Rigid 650 [15].

Property	**Unit**	**Value**
Young's modulus	GPa	0.67 ± 0.06
Ultimate tensile strength	MPa	34 ± 3.4
Elongation at break	%	170 ± 17
Density	G cm^{-3}	1.16
Notched Izod	J m^{-1}	375

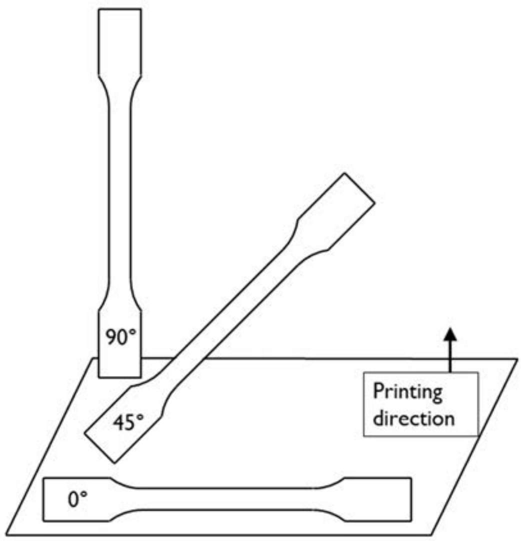

Figure 1: Different investigated printing orientations in respect to print bed.

After the printing, the specimens were washed in a propane-1,2-diyl diacetate (PGDA) bath and cured in an oven at a temperature of 46°C and a relative humidity of 70%.

Specimens type B were produced by the same additive manufacturing process as previously described, with a Formlabs Form 3+ and the same material adopted to produce the specimens type A.

A square glass-fibre-reinforced plastic plate with a thickness of 1.5 mm and an edge length of 53 mm was adhesively joined to the top and bottom of specimen B to ensure uniform loading into the specimen during the testing. The structural epoxy adhesive EC-9323 B/A by 3M Company (St. Paul, MN, USA) [16] was used. The adhesive was applied to the plates, which were then joined to the specimen. With weight placed on top of the specimen to ensure bonding, the structure was placed in an oven and cured at 70°C for a duration of 2 hours.

2.2 Static tests

The quasi-static tests were performed on a Zwick Roell GmbH & Co. KG (Ulm, Germany) universal test machine. The tensile tests using specimen A were conducted at a crosshead velocity of 10 mm/min. The strain was recorded using the DIC tool ARAMIS from Zeiss (Oberkochen, Germany), and the displacement of the crosshead was additionally tracked.

The quasi-static tests of specimen B were carried out on a universal test machine of Zwick-Roell with a load cell with a maximum load of 50 kN at a crosshead velocity of 2 mm/min. The displacement was recorded using the DIC tool ARAMIS from Zeiss. The test setup can be seen in Fig. 2(a).

2.3 Dynamic crushing tests

The dynamic testing of specimen type B was performed using a drop tower. The drop tower compromised a double-sided guided drop sled. The total mass of the drop sled including the load cell and impactor was 16 kg. The maximum drop height is 6 m. A load cell with a maximum load of 160 kN was used. The experiment was recorded using a high-speed camera with up to 40 k fps. The force and load were recorded at a rate of 500 k/s. The via displacement measured velocity before impact was 6.1 m/s. The drop sled and impactor are presented in Fig. 2(b).

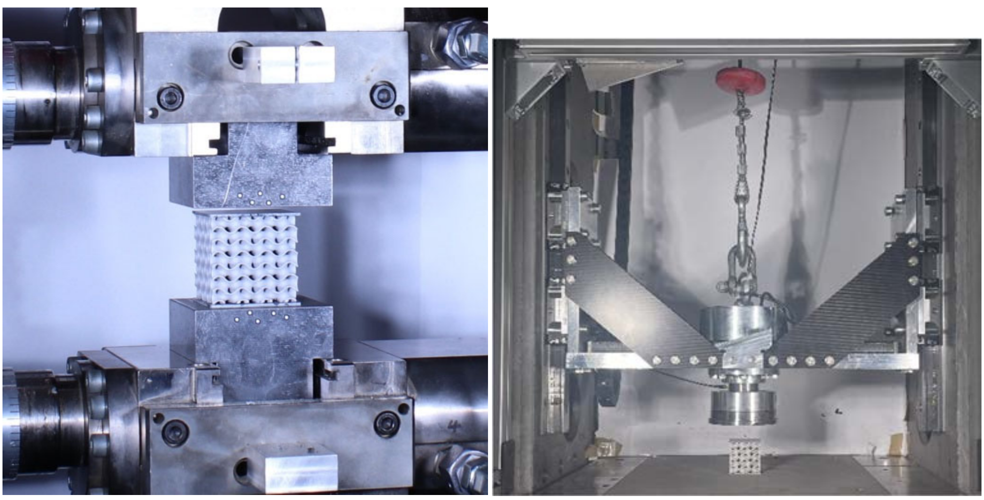

(a) (b)

Figure 2: (a) Test setup of the quasi-static compression on the gyroid specimens; and (b) The dynamic crushing tests on the gyroid specimens.

3 FINITE ELEMENT MODELLING

In this section, the FE modelling methodology is described. First, in Subsection 3.1, the static tests carried out on specimens type A are modelled. Then, in Subsection 3.2, the FE modelling of the quasi-static and crushing tests is presented.

3.1 Material model calibration

The experimental material characterisation is modelled with FE using Simulia/Abaqus Explicit. The dogbone specimen is modelled with C3D8R type elements having characteristic size equal to 1 mm. The specimen was subjected to an imposed displacement at one end, while all the translational and rotational degrees of freedom of the other end were constrained. The model can be observed in Fig. 3. Different hyperelastic material models were compared. Uniaxial test data was provided as input in the material card.

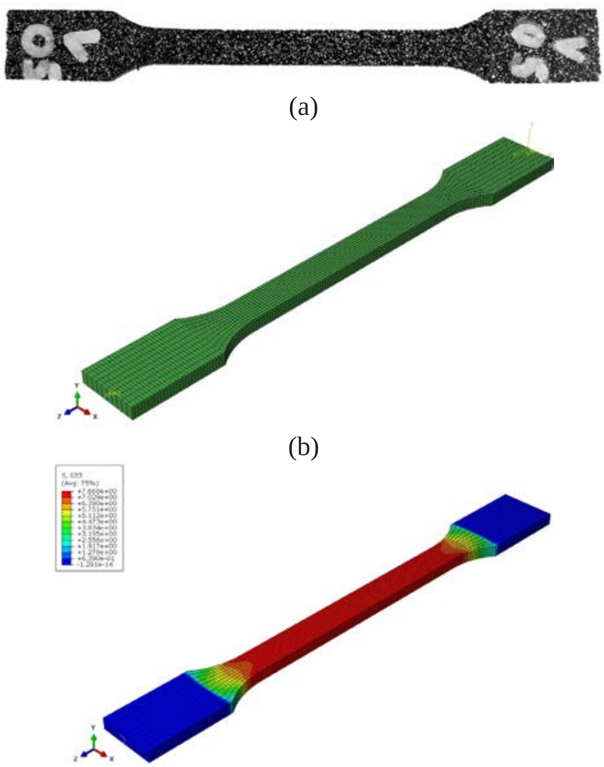

Figure 3: (a) Specimen A in finite element software. The mesh with C3D8 elements (b) and the resulting stress contour (c) are depicted.

3.2 Finite element modelling of triply periodic minimal surface structures

In general, TPMS structures are structures that divide a given volume into two volumes of equal size. This is achieved by an implicit function $\Phi(x,y,z)$ consisting of a combination of sine and cosine function, making the structure periodically duplicable in all three dimensions. An isosurface is generated in all given points where the function of Φ is true. The following equation describes the here investigated gyroid surface [17]:

$$\Phi(x,y,z)=\cos(\lambda_x x)\sin(\lambda_y y)+\cos(\lambda_y y)\sin(\lambda_z z)+\cos(\lambda_z z)\sin(\lambda_x x)=c, \qquad (1)$$

with

$$\lambda_i = 2\pi \frac{n_i}{L_{i,tot}}, \text{ for } i = x, y, z.$$

The appearance of the structure can be adjusted by its total edge length $L_{i,tot}$ and the size of a unit cell n_i. Those two parameters define the periodicity parameter λ_i. The constant c can be varied to shift the dividing isosurface. Additionally, a grading of the structure can be implemented this way. In the most common case, the constant c is zero.

Two distinct methodologies can be used to generate a volumetric structure from this isosurface. On one hand, material can be extruded in one direction perpendicular to the surface, creating a so-called solid network structure. On the other hand, material can be extruded in both directions perpendicular to the surface, generating a so-called sheet network structure. Sheet network structures tend to be isotropic and show greater potential for energy absorption. Therefore, they are the focus of this study. The behaviour and mechanical properties of gyroid structures are dependent on the material, manufacturing process, unit cell size and relative density. The relative density ρ^* is defined as the ratio between the density of the gyroid structure ρ_G and the density of the used material ρ_S.

$$\rho^* = \frac{\rho_G}{\rho_S}. \tag{2}$$

The correlation of the relative density ρ^*, the unit cell size L_i, and the wall thickness d can be approximated by the following equation:

$$d(L_i, \rho^*) = \frac{\rho^* \times L_i^{0,966}}{2.568}. \tag{3}$$

The chosen gyroid configuration is as follows. An edge length of 50 mm is chosen. A unit cell size of 10 mm and a relative density of 17% are selected. Using the above presented equation, a wall thickness of 0.612 mm is defined.

The finite element modelling of the TPMS structure is divided into smaller parts in order to enable a shorter computing time. The mesh generation is conducted in the software Hypermesh by Altair (Troy, MI, USA). The general procedure is as follows. Using the software Matlab R2022b, an .stl file of the isosurface of a gyroid structure is generated. The .stl file is then imported into Hypermesh. Here, the mesh is created and an Abaqus .inp file is created, which can be imported into Abaqus CAE. The mesh is generated using only one unit cell. This unit cell is then divided along all three planes through its centre, creating eight different parts. This enables a more structured mesh. These eight parts are then simultaneously meshed using S4R elements. The wall thickness that was derived above is implemented as the shell thickness. The number of nodes on opposite boundary lines must be equal. Opposing boundary nodes must be mirrored. This unit cell model is used for a mesh convergence study. The base element edge length is varied from 0.1 mm to 1.4 mm. The resulting meshes can be seen in Fig. 4.

The cubic gyroid structure is assembled as well as two rigid plates, which are positioned at the top and bottom of the gyroid structure. The connecting nodes and the given surface of the plate are connected using tie constraints. This is being done to model the adhesive bond between the gyroid structure and the plate in the experimental testing. The deformation is imposed using a smooth step and a displacement of a reference point on the upper plate. The equivalent reference point on the lower plate is pinned.

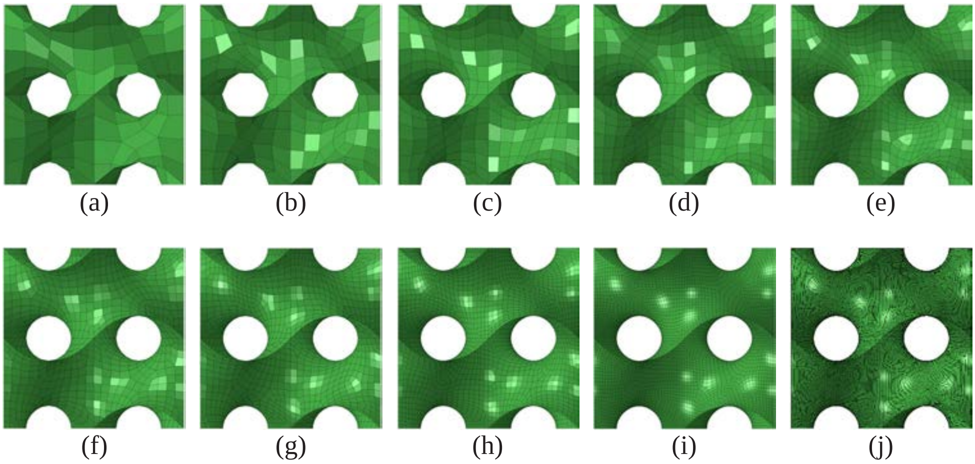

Figure 4: Different mesh sizes of one gyroid unit cell created of an isosurface (shell elements). The unit cell edge length is 10 mm. The mesh is refined from a coarse mesh with element edge lengths of 1.4 mm to a fine mesh. (a) 1.4 mm; (b) 1.2 mm; (c) 1.0 mm; (d) 0.8 mm; (e) 0.6 mm; (f) 0.5 mm; (g) 0.4 mm; (h) 0.3 mm; (i) 0.2 mm; and (j) 0.1 mm.

The large gyroid structure is constructed of five unit cells in each dimension. This is realized in the numerical modelling as follows. One in hypermesh meshed unit cell is imported into the model. This unit cell is then duplicated using the linear pattern function. All coincident nodes are merged, leaving a meshed gyroid structure. This structure is shown in Fig. 5(b). The imposed shell thickness of 0.612 mm is rendered in Fig. 5(c).

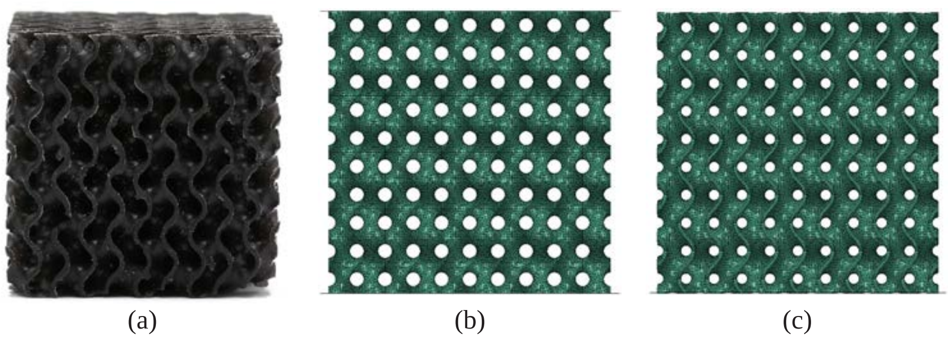

Figure 5: Additively manufactured gyroid structure of PU Rigid 650 material with a relative density of 17% and a unit cell size of 10 mm (a) as well as the numerical modelling of the same structure with shell elements (b). For better visualisation, the imposed shell thickness is rendered (c).

4 RESULTS

4.1 Calibration of the material model with standard dogbone specimens

The results of the experimental testing of specimen A are presented in Fig. 6 in regard to the printing orientation. A mean tensile modulus of 610 MPa was determined. After an initial linear increase in stress, the stress increase is lowered. The stress stays nearly constant over a large increase in strain. Towards the failure of the specimen, the stress increases again. The generated data is used to derive input data for the hyperelastic material model used in the FE modelling (Fig. 6).

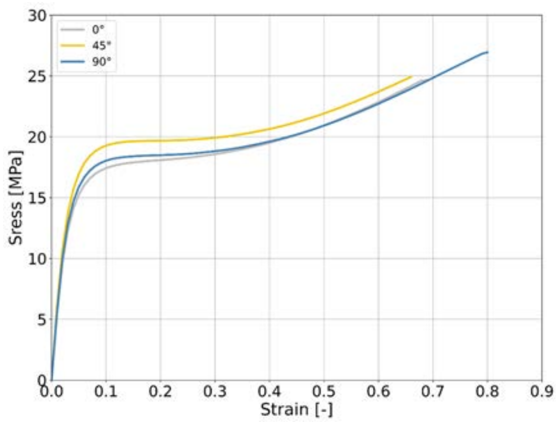

Figure 6: Results of tensile tests. All results of specimens manufactured in the same orientation are compromised into one graph for better comparison.

Overall, it can be observed that the models exhibiting a better numerical–experimental correlation are the ones based on the Ogden and Marlow model (Fig. 7). The result obtained with the Marlow model is however trivial, since such model is not parametric and does not rely on calibration coefficients. On the contrary, the model satisfies the condition for each given point in the calibration, and for any condition in between it interpolates between the two nearest points.

The Ogden model is a type of hyperelastic model describing the nonlinear stress–strain behaviour of materials, which is particularly useful to model polymeric materials, and in particular rubbers. A strain energy potential is defined on the basis of the principal stretches λ, as in eqn (4).

$$W = \sum_{p=1}^{N} \frac{\mu_p}{\alpha_p} \times \left(\lambda_1^{\alpha_p} + \lambda_2^{\alpha_p} + \lambda_3^{\alpha_p} - 3\right), \tag{4}$$

where μ, α and N represent material constants. The principal stress components can be obtained deriving the strain energy potential W with respect to the principal stretch components, as in eqn (5):

$$\sigma_j = -p + \lambda_j \times \frac{dW}{d\lambda_j}, \tag{5}$$

where p represents a Lagrange multiplier enforcing the incompressibility constraint.

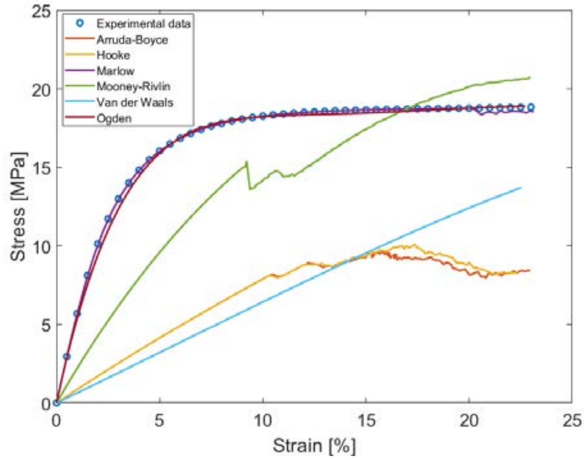

(a)

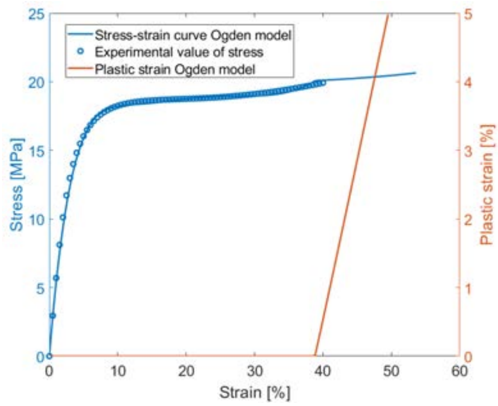

(b)

Figure 7: (a) Stress–strain curves of different hyperelastic material models with the given test input data; and (b) Detailed Ogden model with plastic strain function in regard to total strain.

4.2 Numerical–experimental comparison of static tests

The results of the mesh convergence study, which was conducted under quasi-static compression are presented in Fig. 8. It can be seen that the force–displacement curve converges with smaller element size. The initial peak force is the greatest with an element size of 1.4 mm and decreases with smaller element size. Starting at an element size of 0.5 mm and smaller, the force peak stays nearly constant. The behaviour after the initial failure varies with the element size and is influenced by element deletion of the failed elements. This result indicates that a general element size of 0.5 mm for a 10 mm gyroid unit cell or an element size of 5% of the unit cell length is sufficient to replicate the result achieved with a much finer mesh.

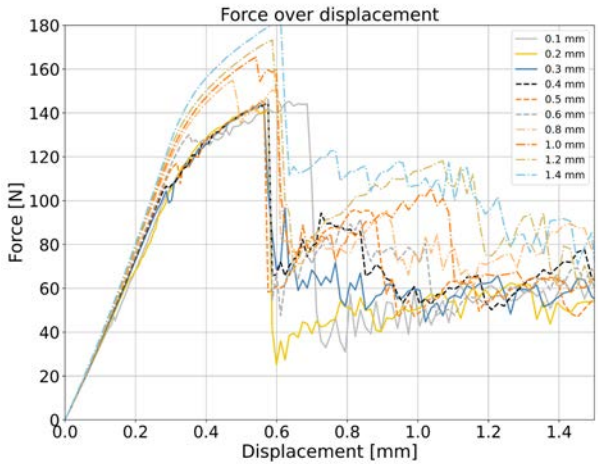

Figure 8: Results of mesh convergence study. The element size of the mesh is indicated in the legend. A sufficient convergence can be observed for an element size of 0.5 mm and smaller.

The result of the simulation of the whole gyroid structure compared to the experimental test is shown in Fig. 9. It can be seen that the numerical data closely follows the obtained force–displacement curve from the experiment. It slightly overestimates the curve. This can be caused by the fact that the material was modelled as isotropic but there were small differences between the specimens of different printing orientations. Additionally, there may have been some manufacturing induced inhomogeneities. When removing the structure from the plate, the specimen may have been damaged.

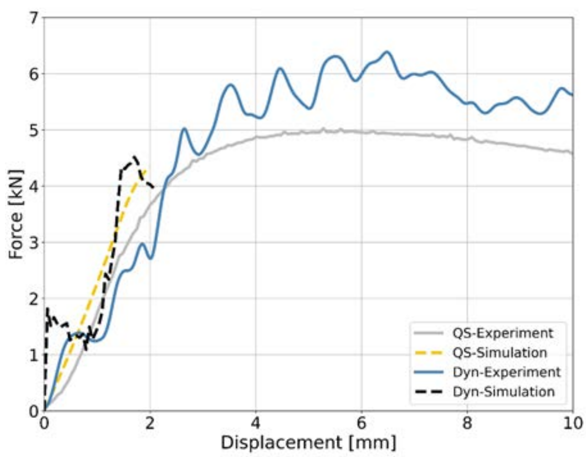

Figure 9: Comparison of experimental and numerical results of compression and crushing tests of a gyroid structure.

www.witpress.com, ISSN 1743-3509 (on-line)

4.3 Numerical–experimental comparison of crushing tests

The results of the dynamic testing and numerical investigation of the specimen type B are presented in Fig. 9. The comparison of the numerical and experimental investigations of the quasi-static and dynamic testing is similar. The force is slightly overestimated. However, a general behaviour of the structure could be obtained for a small displacement. Although the oscillating behaviour of the dynamically tested structure, the dynamic curve is above the quasi-static one, most likely due to its strain rate sensitivity. Though, the simulations were aborted prematurely due to distorted elements on the boundaries, the initial slope is sufficiently captured from both the static and dynamic analysis.

5 CONCLUSIONS

In this experimental and numerical study, a recently available photopolymer for energy absorption applications has been investigated. In connection with a TPMS gyroid structure, this material can potentially be used for lightweight energy absorbing structures, e.g. a wing leading edge for bird strike loading. Therefore, a hyperelastic Ogden material model with plasticity was found to correctly reproduce the material behaviour. This material model was then implemented in a cubic gyroid structure of five unit cells of 10 mm length, resulting in a cubic structure with an edge length of 50 mm. This method showed to be promising for the applicability on real world structures. Future works will be aimed at validating this approach in order to demonstrate the applicability to represent typical aeronautical elements.

ACKNOWLEDGEMENT

We would like to acknowledge the funding by the Deutsche Forschungsgemeinschaft (DFG, German Research Foundation) under Germany’s Excellence Strategy – EXC 2163/1 – Sustainable and Energy Efficient Aviation – Project-ID 390881007.

REFERENCES

[1] Lobitz, L. et al., Aircraft wing design for extended hybrid laminar flow control. *Aerospace*, **10**(11), p. 938, 2023.
[2] Traub, H., Wolff, J., Jose, S., Lobitz, L., Schollerer, M. & Hühne, C., Concept and design of extended hybrid laminar flow control suction panels, 2021. https://doi.org/10.21203/rs.3.rs-924184/v1.
[3] Beck, N., Landa, T., Seitz, A., Boermans, L., Liu, Y. & Radespiel, R., Drag reduction by laminar flow control. *Energies*, **11**(1), p. 252, 2018.
[4] Terrenoire, E., Hauglustaine, D.A., Gasser, T. & Penanhoat, O., The contribution of carbon dioxide emissions from the aviation sector to future climate change. *Environmental Research Letters*, **14**(8), 084019, 2019.
[5] Giannakeas, I.N., Khodaei, Z.S. & Aliabadi, M.F., Structural health monitoring cost estimation of a piezosensorized aircraft fuselage. *Sensors*, **22**(5), p. 1771, 2022.
[6] Wiedemann, M. et al., The suction panel-xHLFC and structural solution for energy efficient aviation. *AIAA Scitech 2022 Forum*, p. 0007, 2022.
[7] Zhang, L., Feih, S., Daynes, S., Chang, S., Wang, M.Y., Wei, J. & Lu, W.F., Energy absorption characteristics of metallic triply periodic minimal surface sheet structures under compressive loading. *Additive Manufacturing*, **23**, pp. 505–515, 2018.
[8] Sun, Q., Sun, J., Guo, K. & Wang, L., Compressive mechanical properties and energy absorption characteristics of SLM fabricated Ti6Al4V triply periodic minimal surface cellular structures. *Mechanics of Materials*, **166**, 104241, 2022.

[9] Yu, S., Sun, J. & Bai, J., Investigation of functionally graded TPMS structures fabricated by additive manufacturing. *Materials and Design*, **182**, 108021, 2019.

[10] Novak, N., Al-Ketan, O., Krstulović-Opara, L., Rowshan, R., Al-Rub, R.K.A., Vesenjak, M. & Ren, Z., Quasi-static and dynamic compressive behaviour of sheet TPMS cellular structures. *Composite Structures*, **266**, 113801, 2021.

[11] Wang, H., Tan, D., Liu, Z., Yin, H. & Wen, G., On crashworthiness of novel porous structure based on composite TPMS structures. *Engineering Structures*, **252**, 113640, 2022.

[12] Qiu, N., Wan, Y., Shen, Y. & Fang, J., Experimental and numerical studies on mechanical properties of TPMS structures. *International Journal of Mechanical Sciences*, **261**, 108657, 2024.

[13] Ma, X., Zhang, D.Z., Yu, X., Ren, Z., Mao, S. & Zheng, X., A novel design method for TPMS lattice structures with complex contour based on moving elements method. *The International Journal of Advanced Manufacturing Technology*, **123**(1), pp. 21–33, 2022.

[14] DIN Deutsches Institut für Normung e.V., Plastics: Determination of tensile properties. Deutsche Norm – DIN EN ISO 527-2. Beuth Verlag GmbH: Berlin, Germany, 2012.

[15] Formlabs, PU Rigid 650: For impact resistant and semi-stiff polyurethane parts. Formlabs: Somerville, MA, USA, 2022.

[16] 3M Company, 3MTM Scotch-WeldTM Structural Epoxy Adhesive EC-9323 B/A. Technical Data Sheet. 3M Company: Saint Paul, MN, USA, 2022.

[17] Schoen, A.H., Infinite periodic minimal surfaces without self-intersections. Technical Note NASA TN D-5541. National Aeronautics and Space Administration: Washington, DC, USA, 1970.